Dispersion and thermal effects on electromagnetic instabilities in the precursor of relativistic shocks

Martin Lemoine, Guy Pelletier

Monthly Notices
of the
ROYAL ASTRONOMICAL SOCIETY

Mon. Not. R. Astron. Soc. **417,** 1148–1161 (2011) doi:10.1111/j.1365-2966.2011.19331.x

Dispersion and thermal effects on electromagnetic instabilities in the precursor of relativistic shocks

Martin Lemoine[1⋆] and Guy Pelletier[2⋆]

[1]*Institut d'Astrophysique de Paris, CNRS, UPMC, 98 bis boulevard Arago, F-75014 Paris, France*
[2]*Laboratoire d'Astrophysique de Grenoble, CNRS, Université Joseph Fourier II, BP 53, F-38041 Grenoble, France*

Accepted 2011 June 27. Received 2011 May 11; in original form 2011 February 16

ABSTRACT

Fermi acceleration can develop efficiently at relativistic collisionless shock waves provided the upstream (unshocked) plasma is weakly magnetized. This has been both indicated by analytical theory and observed in numerical particle-in-cell simulations. At low magnetization, the large size of the shock precursor indeed provides enough time for electromagnetic micro-instabilities to grow, and such micro-instabilities generate small-scale turbulence that in turn provides the scattering required for particles to undergo Fermi cycles at superluminal relativistic shock waves. The present paper extends our previous analysis on the development of these micro-instabilities to account for the finite angular dispersion of the beam of reflected and accelerated particles and to account for the expected heating of the upstream electrons in the shock precursor. Indeed, we argue that the electrons can be significantly heated during their travel in the shock precursor and that they may even reach equipartition with protons, in agreement with recent numerical simulations. We show that the oblique two-stream instability may operate down to values of the shock Lorentz factor $\gamma_{\rm sh} \sim 10$ (corresponding to a relatively large angular dispersion of the beam) as long as the electrons of the upstream plasma remain cold, while the filamentation instability is strongly inhibited in this limit; however, as electrons get heated to relativistic temperatures, the situation becomes opposite and the two-stream instability becomes inhibited while the filamentation mode becomes efficient, even at moderate values of the shock Lorentz factor. The peak wavelength of these instabilities migrates from the inertial electron scale towards the proton inertial scale as the background electrons get progressively heated during the crossing of the shock precursor. We also discuss the emergence and the role of current-driven instabilities upstream of the shock. In particular, we show that the returning and accelerated particles give rise to a transverse current through their rotation in the background magnetic field. We find that the compensating current in the background plasma can lead to a Buneman instability which provides an efficient source of electron heating.

Key words: acceleration of particles – shock waves – cosmic rays.

1 INTRODUCTION

The acceleration of particles through repeated interactions with the electromagnetic fields up- and downstream of a collisionless shock front is generally taken as the source the non-thermal particle populations that are detected in powerful astrophysical outflows. The physics of this Fermi mechanism is relatively well understood for non-relativistic shock velocities, at least in the test particle limit in which one neglects the backreaction of the accelerated particles on the shock environment. In the relativistic limit however, in which the shock moves towards the upstream (unshocked) medium with a bulk Lorentz factor $\gamma_{\rm sh} \gg 1$, the situation becomes more intricate, mostly because the shock now moves about as fast as the accelerated particle. In non-relativistic shocks one can distinguish the details of the shock structure from that of the Fermi process, as this latter takes place on spatial scales much larger than the shock thickness. In contrast, in relativistic shocks, the structure of the shock plays a significant role in the Fermi process and in the process of generation of the electromagnetic turbulence. One important issue, in particular, is the reflection of a part of the cold upstream particles at the shock front, which together with the Fermi accelerated particles travels back upstream and initiate instabilities in the upstream plasma.

These instabilities play a key role in the development of the Fermi process and, consequently, in the radiative signatures of

⋆E-mail: lemoine@iap.fr (ML); guy.pelletier@obs.ujf-grenoble.fr (GP)

relativistic outflows. Indeed, at magnetized oblique ultra-relativistic shock waves, the Fermi process may develop only if sufficient micro-turbulence has been generated in order to prevent the advection of the accelerated particles away from the shock front into the far downstream plasma (Begelman & Kirk 1990; Niemiec & Ostrowski 2006; Lemoine, Pelletier & Revenu 2006). Moreover, for the vast majority of them, ultra-relativistic shock waves are oblique: the opposite parallel configuration only takes effect when the magnetic field lines are oriented to an angle with the shock normal smaller than $1/\gamma_{\rm sh}$ (in the unshocked plasma or upstream rest frame). As to the meaning of 'magnetized' shock waves, it is slightly ambiguous and context-dependent; above, it is meant: with a pre-existing (upstream) magnetic field $B_{\rm u}$ such that, after compression through the shock and Lorentz transform into the downstream frame, the typical Larmor radius of accelerated particles is much smaller than the width of the blast, which is of the order of $R/\gamma_{\rm sh}$ in this frame (R denotes the shock radius). For smaller values of $B_{\rm u}$, the accelerated particles can explore the whole blast and beyond, hence they may scatter on magnetic inhomogeneities sourced elsewhere, which would allow their repeated interactions with the shock. Nevertheless, for such low values of $B_{\rm u}$, the generation of micro-turbulence is almost guaranteed, as will be discussed in the following; hence the Fermi process should develop independently of any extra source of magnetic inhomogeneities.[1] Furthermore, there exist evidence for amplification of the magnetic field upstream of a relativistic shock [see e.g. Li & Waxman (2006) and Li & Zhao (2011), which can be seen as a hallmark of the development of micro-instabilities upstream of the shock].

On microscopic plasma scales, several instabilities may develop in the precursor of the shock front through the penetration of the beam of returning and accelerated particles into the upstream plasma. The filamentation instability in particular – often referred to as the Weibel instability in the literature – has been proposed as the agent of amplification of the magnetic field to the level inferred from the synchrotron interpretation of gamma-ray burst afterglows (Gruzinov & Waxman 1999; Medvedev & Loeb 1999; see also Wiersma & Achterberg 2004; Lyubarsky & Eichler 2006; Achterberg & Wiersma 2007; Achterberg, Wiersma & Norman 2007). Recently, it has been found that the growth rate of two-stream instabilities in an oblique configuration (Bret, Firpo & Deutsch 2005a) is larger than that of the filamentation mode (Bret 2009; Lemoine & Pelletier 2010). Which instability grows faster is a key question here, as the relativistic velocity of the shock wave and the level of upstream magnetization strongly limit the penetration length-scale of the accelerated particles into the upstream plasma before these particles are caught back by the shock wave (Milosavljević & Nakar 2006; Pelletier et al. 2009); and as mentioned before, if such instabilities cannot grow, then Fermi acceleration cannot develop (at least, in the absence of extra sources of turbulence).

The detailed conditions under which the above instabilities and other relevant modes can grow, together with the development of Fermi cycles as a function of the shock velocity and the upstream magnetization, have been discussed in a previous paper (Lemoine & Pelletier 2010). That paper assumed a charge neutralized beam without angular dispersion propagating in a cold background plasma. It is the aim of the present paper to revisit these assumptions and to extend the previous calculations to a more generic situation, in which the beam angular dispersion (which is fixed by kinematics, as discussed below) is taken into account, and in which the effects of heating of the upstream plasma are considered. The emergence of current instabilities is also discussed. The present study is warranted in particular by recent work (Lyubarsky & Eichler 2006; Rabinak, Katz & Waxman 2011) that showed that the small opening angle of the beam suffices to prevent the onset of the filamentation instability in electron–proton plasmas of shock Lorentz factor $\gamma_{\rm sh} \lesssim 100$, independently of the length-scale of the precursor. The present study recovers this result for a cold background plasma, but it also argues that: (i) the two-stream instability and more precisely its oblique mode version are less sensitive to the beam angular dispersion as it can develop down to $\gamma_{\rm sh} \sim 10$ in the same conditions; (ii) the heating of the background plasma has a major effect in that it may help sustain the development of instabilities down to $\gamma_{\rm sh} \sim 10$.

This paper is organized as follows. In Section 2, we first review the current understanding on the structure of the shock, relying on the results of the most recent particle-in-cell (PIC) simulations of relativistic collisionless shocks. We also discuss in a general way the instabilities that may develop as a function of the two main characteristics of the shock: upstream magnetization and shock velocity. In Section 3, we then discuss how the filamentation and two-stream instabilities are affected by the finite angular dispersion of the beam of returning particles, assuming the background plasma to remain cold. In Section 4, we generalize the calculations of Section 3 to a background plasma composed of cold protons and relativistically hot electrons. Finally, in Section 5 we discuss the possibility of current instabilities and their role in shaping the precursor. We summarize our results and draw conclusions in Section 6. In Appendix A, we explicit the susceptibility tensor of the beam of finite angular dispersion, modelled with a waterbag distribution in the transverse momentum direction (transverse with respect to the shock normal) and a Dirac distribution in the parallel momentum direction.

2 GENERAL CONSIDERATIONS

2.1 Shock structure and precursor

Let us first describe the general structure of a relativistic collisionless shock and introduce the main quantities of interest for the present discussion.

The shock is characterized by a small number of parameters: (i) the composition ahead of the shock front, in the upstream plasma – in what follows, we assume except otherwise noted that the plasma is composed of electrons and protons with densities $n_{\rm e} = n_{\rm p} \equiv n_{\rm u}$; (ii) the equation of state of the upstream plasma, which will be taken cold or composed of relativistically hot electrons but cold protons (see also further below for more details on this point); (iii) the shock velocity, written as $\beta_{\rm sh}c$ as measured in the upstream frame, with corresponding Lorentz factor $\gamma_{\rm sh}$; (iv) the magnetization of the upstream plasma, written as $\sigma_{\rm u}$ and defined as

$$\sigma_{\rm u} \equiv \frac{B_{\rm u}^2}{4\pi n_{\rm u} m_{\rm p} c^2} \,. \tag{1}$$

The magnetic field strength $B_{\rm u}$ is here measured in the upstream frame. The shock structure also depends on the obliquity of the background magnetic field, but in what follows and except otherwise noted, we will focus on the generic superluminal case in which the

[1] More generally speaking, Fermi acceleration requires micro-turbulence to be generated at distances smaller than $r_{\rm L,0}$, with $r_{\rm L,0}$ the Larmor radius in the downstream frame shock compressed background magnetic field (Pelletier, Lemoine & Marcowith 2009). While this is guaranteed for micro-instabilities when they can be triggered in the precursor, this constraint can be turned into a lower bound on the growth rate of extra sources of turbulence, which of course differs from the constraint on the growth of micro-instabilities discussed here and in Lemoine & Pelletier (2010).

angle with respect to the shock normal exceeds $1/\gamma_{\rm sh}$. Then, in the shock front rest frame, the magnetic field lies mostly perpendicular to the flow direction, as the transverse components are amplified by a factor $\gamma_{\rm sh}$ while the parallel component remains unchanged by the Lorentz transform. For an oblique shock wave, the above magnetization parameter thus measures (up to a $\sin^2\Theta_B \sim 1$ factor, with Θ_B the angle between the shock normal and the magnetic field in the upstream rest frame) the ratio of the magnetic energy in the shock front frame relative to the incoming matter flux $\gamma_{\rm sh}^2 n_{\rm u} m_{\rm p} c^2$ crossing the shock front.

Collisionless shock waves can be mediated by three generic types of mechanisms: by an electrostatic potential for incoming protons in an $e-p$ shock, by a magnetic barrier or, if the magnetic field is negligible, by a reflection due to the ponderomotive force of growing waves ahead of the shock transition layer. In the case of the external shock of a gamma-ray burst outflow propagating in the interstellar medium, for example, the reflection can take place on a potential barrier or through a ponderomotive force, as the ambient magnetic field is then particularly weak, $\sigma_{\rm u} \sim 10^{-9}$ for $B_{\rm u} \sim 1\,\mu$G and $n_{\rm u} \sim 1\,{\rm cm}^{-3}$. However, even weak, the ambient magnetic field can play an important role, as will be seen further on.

The magnetic field at a relativistic shock front is associated with a motional electric field $E_{\rm u|sh} = \beta_{\rm sh} B_{\rm u|sh}$ when measured in the shock front frame (as indicated by the $_{\rm |sh}$ subscript), with $B_{\rm u|sh} \simeq \gamma_{\rm sh} B_{\rm u}$ (again, up to a factor $\sin\Theta_B$). Since the magnetic field is frozen in most parts of the plasma, the transverse component is further increased by the velocity decrease as the upstream incoming plasma approaches the shock transition layer, as seen again in the shock front rest frame. This magnetic barrier may reflect back a fraction of the incoming protons. In the strongly magnetized case, $\sigma_{\rm u} \gtrsim 0.1$, the coherent gyration of the incoming protons and electrons gives rise to the emission of large amplitude electromagnetic waves through the synchrotron maser instability (Langdon, Arons & Max 1988). As these waves travel back upstream, they lead to a form of wakefield acceleration of the electrons, which leads to electron heating at the expense of the incoming protons (Lyubarsky 2006; Hoshino 2008).

The rise of an electrostatic barrier can be described as follows. To reach thermalization through the shock transition layer, the electrons need to absorb part of the wave energy, possibly through a kind of anomalous Joules heating. Whatever the mechanism, the length required for the electron heating is several inertial length $\delta_{\rm e} \equiv c/\omega_{\rm pe}$, much smaller than the length-scale of the precursor. As electrons remain approximatively in Boltzmann equilibrium, their density increase in the shock transition by a compression factor r is accompanied by a potential variation $\Delta\Phi$ such that $e\Delta\Phi \sim T_{\rm e} \ln r$. If the electrons are heated to equipartition with the protons in the downstream plasma, their temperature $T_{\rm e} \sim T_{\rm p} \sim \gamma_{\rm sh} m_{\rm p} c^2$ in the downstream plasma. In an electron–proton shock, it thus seems unavoidable to have a potential barrier that reflects part of the incoming protons (see also Gedalin, Balikhin & Eichler 2008); this is an important difference with an electron–positron plasma.

If intense waves are excited in the precursor by the reflected particles or by emitted electromagnetic waves, their growth may also reflect part of the particles, notably electrons. In particular, such a mechanism is warranted to ensure the shock transition in an unmagnetized pair plasma, as evidenced by various PIC simulations (see e.g. Spitkovsky 2008b).

The composition of the beam of returning particles is an important issue with respect to the development of instabilities in the upstream plasma, in particular whether charge neutralization has been achieved or not. In that respect, it should be noted that, if electrons are heated to near equipartition with the incoming protons in the shock precursor, the shock itself must behave as if it were a pair shock. Then, the electrostatic barrier can be expected to be negligible and the returning beam is essentially charge neutralized.

Whether and to what amount the electrons are heated in the shock precursor depend in turn on the instabilities that are generated in this precursor. Let us denote by $\chi_{\rm e} \leq 1$ the fraction of the incoming (proton) energy carried by the electrons as they reach the shock transition layer. Then, $\chi_{\rm e} = m_{\rm e}/m_{\rm p}$ if the electrons have not been heated in the precursor, and $\chi_{\rm e} = 1$ if equipartition with the ions has been reached. This parameter $\chi_{\rm e}$ is now measured by massive PIC simulations (Spitkovsky 2008a; Sironi & Spitkovsky 2009, 2011): generally speaking, it is found that $\chi_{\rm e} \sim 1$ for strongly magnetized plasmas, $\chi_{\rm e} < 1$ in the intermediate magnetization regime $\sigma_{\rm u} \sim 10^{-4}$ to 10^{-2} and $\chi_{\rm e}$ rises up to unity again at lower magnetizations.

As discussed in Lemoine & Pelletier (2010), the returning protons and the first generation of accelerated particles form a forward beam of energy $\gamma_{\rm sh}^2 m_{\rm p} c^2$. In the following, we write $\gamma_{\rm b} = \gamma_{\rm sh}^2$ the Lorentz factor of the protons composing the beam. If the electrons composing the beam have been heated to equipartition with the protons before being reinjected towards upstream, either through reflection or through shock crossing from downstream toward upstream, they carry a same energy $\gamma_{\rm sh}^2 m_{\rm p} c^2$ hence their beam plasma frequency is also similar.

In the precursor, the trajectory of a reflected proton is a cycloid with an extension upstream that determines the width of the 'foot' region (i.e. the precursor) $\ell_{\rm f|sh} = \gamma_{\rm sh} m_{\rm p} c^2/eB_{\rm u|sh}$ (measured in the shock front rest frame). As measured in the upstream frame, this length-scale $\ell_{\rm f|u} = \ell_{\rm f|sh}/\gamma_{\rm sh}$; this corresponds to $r_{\rm L|u}/\gamma_{\rm sh}^3$ with a Larmor radius $r_{\rm L|u} = \gamma_{\rm sh}^2 m_{\rm p} c^2/eB_{\rm u}$; the factor $\gamma_{\rm sh}^3$ comes from the fact that the reflected protons are caught up by the shock front after having travelled along the Larmor circle only $r_{\rm L|u}/\gamma_{\rm sh}$ before being caught back by the shock front (Gallant & Achterberg 1999; Achterberg et al. 2001), keeping in mind that the distance between the particle and the front is reduced by a factor $1-\beta_{\rm sh} \simeq 1/(2\gamma_{\rm sh}^2)$ (Milosavljević & Nakar 2006; Pelletier et al. 2009).

When the Fermi process develops through cycles of particles crossing the front back and forth, the first cycle always occurs and the particles participating in this first cycle have an energy comparable to that of the reflected protons. One can thus assimilate the reflected protons to those first cycle particles, and the number of particles involved in the Fermi process will only slightly increase with further cycles. We will note $\xi_{\rm b}$ the ratio of the incoming energy density converted into the pressure of these supra-thermal particles:

$$\xi_{\rm b} \equiv \frac{n_{\rm b} m_{\rm p} c^2}{\gamma_{\rm sh} n_{\rm u} m_{\rm p} c^2}, \tag{2}$$

and $n_{\rm b}$ denotes the proper density of the beam particles (i.e. measured in the shock front rest frame). This parameter $\xi_{\rm b}$ approximately corresponds to the ratio of the supra-thermal particle density over the upstream particle density measured in this same shock rest frame.

2.2 Instabilities at a relativistic collisionless shock

In the case of a current neutralized charged beam, meaning a beam carrying positive and negative charges but zero net current along the shock normal, the leading instabilities at small magnetization are the filamentation mode, the two-stream instabilities, in particular the Čerenkov resonance mode with electrostatic modes (or with

modes of wavenumber parallel to the magnetic field in the case of a magnetized plasma) or with Whistler modes (for an electron–proton plasma). The filamentation instability takes place at small real frequencies $\mathcal{R}\omega \sim 0$ and small parallel wavenumber $k_\parallel \ll k_\perp$ relatively to the transverse wavenumbers (parallel and transverse are defined relatively to the shock normal), while the two-stream electrostatic instability takes place at resonance $\mathcal{R}\omega \simeq \omega_\mathrm{p}$, $k_\parallel \simeq \omega_\mathrm{p}/c$ in the upstream rest frame, with $\omega_\mathrm{p} = (4\pi n_\mathrm{u} e^2/m_\mathrm{e})^{1/2}$ the background plasma frequency.

Such charge-driven current neutralized instabilities are of course generic in the case of pair shocks. However, even in that case, one must expect a transverse current to rise at the tip of the precursor, as a consequence of charge splitting in the external magnetic field. This current then generates a compensating current in the background plasma, which induces a Buneman instability, which itself leads to efficient heating of the background electrons in the shock precursor. This issue will be addressed in Section 5.

In the case of an electron–proton plasma, the beam can be current neutralized if, as mentioned above, the incoming upstream electrons are preheated to near equipartition with the protons during the crossing of the precursor; then, for all practical matters, the shock transition resembles that of a pair shock and the returning beam carries a vanishing current. Of course, in that case as well, one expects the transverse current to emerge in a magnetized upstream plasma and give rise to a Buneman type instability (see Section 5). As mentioned before, such near equipartition has been observed in PIC simulations in both the high and low magnetization limits in oblique collisionless shock waves (Sironi & Spitkovsky 2011). At high magnetization, electron heating in the precursor is due to wakefield acceleration associated with the ponderomotive force of the large amplitude waves emitted by the synchrotron maser instability (Lyubarsky 2006; Hoshino 2008). At low magnetization, electron heating appears to be related to the development of micro-instabilities in the shock precursor.

Such micro-turbulent heating can be understood as follows. Consider for simplicity the fully unmagnetized limit and select the upstream rest frame; assume further that the shock has reached a stationary state. The micro-turbulence is excited on a length-scale $\ell'_{\mathrm{f|u}}$ that differs from the previous value of the foot length $\ell_{\mathrm{f|u}}$, as we now neglect any pre-existing magnetic field and assume that scattering is dominated by the micro-turbulence (see Milosavlejvić & Nakar 2006; Pelletier et al. 2009). The magnitude of this length-scale is such that the transverse momenta of returning particles diffuse by an amount $\langle \Delta p^2_{\mathrm{b},\perp} \rangle \sim {p_\mathrm{b}}^2/\gamma^2_\mathrm{sh}$ during their travel time $2\gamma^2_\mathrm{sh}\ell'_{\mathrm{f|u}}/c$ in this precursor. The prefactor $2\gamma^2_\mathrm{sh}$ corresponds, as before, to the difference between the return time-scale of the accelerated particles and the precursor light crossing time. For returning/accelerated particles, the momentum $p_\mathrm{b} \sim \gamma^2_\mathrm{sh} m_\mathrm{p} c$. Diffusion of momenta takes place through scatterings on small (plasma) scale electromagnetic fields. Such small-scale fields equally contribute to heating the upstream plasma electrons, provided that the electric wave energy content is not much smaller than its magnetic counterpart. However, the upstream electrons only experience the length-scale $\ell'_{\mathrm{f|u}}$ during a light crossing time $\ell'_{\mathrm{f|u}}/c$. Consequently, their momentum dispersion amounts to $\Delta p^2_\mathrm{u} \sim {m_\mathrm{p}}^2 c^2/2$ once the electrons reach the shock front, which corresponds to equipartition with the incoming ions.

To go one step further, one can easily conceive that the preheating of the electrons to near equipartition in the precursor provides the only means to achieve near neutralization of the returning particle current. If indeed electrons are not preheated in the precursor but simply overturned (by, say, the micro-turbulence), their Lorentz factor is increased by a factor γ^2_sh but their energy remains a factor $m_\mathrm{e}/m_\mathrm{p}$ below that of the returning proton beam. Consequently, their penetration length-scale is also a factor $m_\mathrm{e}/m_\mathrm{p}$ smaller and, for all relevant purposes, the beam can be considered as essentially composed of protons.

In short, a net current along the shock normal in the upstream plasma may arise if and only if the electrons have not been heated to equipartition with the incoming ions by the time they reach the shock front. According to the recent PIC simulations of Sironi & Spitkovsky (2011), parallel shock waves offer such an example in which the electrons reach the shock transition with an energy that is significantly less than that of the protons. It is then natural to expect current instabilities, such as the Bell (2004) instability – more exactly, its relativistic generalization (see Reville, Kirk & Duffy 2006) – to develop in the upstream plasma (Lemoine & Pelletier 2010). This will be discussed in Section 5.

In Sections 3 and 4, we concentrate on the filamentation and two-stream instabilities and we discuss their development once the finite angular dispersion of the beam of accelerated particles has been taken into account, and considering the possibility that the electrons of the background (upstream) plasma have been preheated through the micro-turbulence to relativistic temperatures. Following the approximation scheme discussed in our previous paper (Lemoine & Pelletier 2010), we consider the micro-instabilities triggered in the ambient plasma by the returning beam over a length-scale that is limited by a low background magnetization. In that paper, which discussed the instabilities under the assumption of a unidirectional beam and a cold ambient plasma, we showed that the Weibel-filamentation instability and the oblique two-stream instability in particular are very weakly modified by the magnetic field during their linear growth, notably because the maximum length-scale of the precursor is always much smaller than the Larmor radius of the beam. Moreover the magnetization of the ambient plasma is always assumed much smaller than unity. Thus, in this paper, we neglect the contribution of the magnetic field to the dispersion tensor. Of course, such a contribution cannot be neglected when discussing the development of Whistler waves. However we do not consider such an instability in the present paper as one of our conclusions is that upstream electrons are heated towards equipartition, which quenches the development of Whistler waves.

3 INSTABILITIES WITH A COLD BACKGROUND PLASMA AND FINITE BEAM ANGULAR DISPERSION

3.1 Beam geometry

Henceforth, we consider a current neutralized beam composed of electrons and protons moving with bulk Lorentz factor γ_b in the upstream rest frame. In this section, we furthermore assume the background plasma to be cold.

We model the beam with the following axisymmetric waterbag distribution function:

$$f_\mathrm{b}(\boldsymbol{u}) = \frac{1}{\pi u^2_\perp}\delta(u_x - u_\parallel)\Theta\left(u^2_\perp - u^2_y - u^2_z\right), \tag{3}$$

introducing the velocity variables $u_i = p_i/(mc)$, where p_i denotes the i-component of the beam momentum. The beam thus propagates towards $+x$ (parallel direction) and suffers from angular dispersion in the perpendicular plane, as characterized by the ratio $u_\perp/u_\parallel$.

In the case of particles returning from or through a relativistic shock of Lorentz factor γ_sh and propagating in the unshocked

plasma, the amount of angular dispersion is known to be $u_\perp \simeq u_\parallel/\gamma_{\rm sh}$. This result is dictated by kinematics: given that the shock front is always trailing right behind the accelerated particle, once the parallel velocity of this latter drops below $\beta_{\rm sh}$, i.e. once the perpendicular velocity of this latter exceeds $c/\gamma_{\rm sh}$, the particle is caught back by the shock wave (Gallant & Achterberg 1999; Achterberg et al. 2001). As the beam (proton) Lorentz factor $\gamma_{\rm b} \simeq \gamma_{\rm sh}^2$ and $\gamma_{\rm sh} \gg 1$, this implies $u_\perp \ll u_\parallel$, hence $u_\parallel \simeq \gamma_{\rm b}$ and $u_\perp \simeq \gamma_{\rm sh} \simeq \sqrt{\gamma_{\rm b}}$. This hierarchy allows us to calculate the susceptibility tensor of the beam by neglecting in a systematic way u_y^2 and u_z^2 in front of u_x^2. Of course, one must pay attention not to neglect u_y, u_z in the poles of the form $\omega - \boldsymbol{k}\cdot\boldsymbol{\beta}c = \omega - k_i u_i c/\gamma_{\rm b}$. The corresponding beam susceptibility tensor $\chi_{ij}^{\rm b}$ is detailed in Appendix A.

In the final expression for $\chi_{ij}^{\rm b}$, the angular dispersion enters through the ratio $k_\perp u_\perp c/R_\parallel$, with $R_\parallel = \gamma_{\rm b}\omega - k_\parallel u_\parallel c$ (see Appendix A). Therefore, its impact on the growth of instabilities is determined by $k_\perp$, $\gamma_{\rm sh}$ and the nature of the instability which determines $R_\parallel$. At the Čerenkov resonance, $R_\parallel \simeq \gamma_{\rm b}\omega_k\delta$, with ω_k the eigenmode pulsation, and δ a complex number of modulus $|\delta| \ll 1$; at leading order, δ is a cubic root of unity in the limit $u_\perp \to 0$ (see Lemoine & Pelletier 2010), hence the growth rate $\mathcal{I}\omega = \omega_k\mathcal{I}\delta \approx |R_\parallel/\gamma_{\rm b}|$ (at resonance). Consequently, the ratio $|k_\perp u_\perp c/R_\parallel| \approx k_\perp\beta_\perp c/\mathcal{I}\omega$. If $k_\perp\beta_\perp c/\mathcal{I}\omega > 1$, the angular dispersion terms dominate over the resonance poles, hence one expects growth to be inhibited. Formally, the beam susceptibility changes structure in this limit, as discussed in Appendix A. Physically, one recovers the argument of Akhiezer (1975) that the particles travel in the perpendicular direction more than one wavelength of the unstable mode on an e-folding time-scale of the instability, hence coherence is lost and growth inhibited, as discussed recently by Rabinak et al. (2011). Another important instability in the precursor of relativistic shocks is the filamentation mode, with $\mathcal{R}\omega \sim 0$, $k_\parallel \ll k_\perp$. Then $k_\perp u_\perp c/R_\parallel \sim k_\perp\beta_\perp c/\mathcal{I}\omega$ as well.

Assuming, as we do in Appendix A, that the transverse component of the wavenumber lies along $\boldsymbol{y}$, the dispersion relation to be solved reads

$$\left(\omega^2 - \omega_{\rm p}^2 - k_\perp^2 + \chi_{xx}^{\rm b}\omega^2\right)\left(\omega^2 - \omega_{\rm p}^2 - k_\parallel^2 + \chi_{yy}^{\rm b}\omega^2\right) - \left(k_\parallel k_\perp + \chi_{xy}^{\rm b}\omega^2\right)^2 = 0. \quad (4)$$

The susceptibility tensor $\chi_{ij}^{\rm b}$ scales as the ratio squared of the beam plasma frequency to the background plasma frequency, i.e.

$$\left(\frac{\omega_{\rm pb}}{\omega_{\rm p}}\right)^2 = \xi_{\rm b}\frac{m_{\rm e}}{m_{\rm p}}, \quad (5)$$

with $\xi_{\rm b}$ defined in equation (2). In the following, we solve numerically the dispersion relation for the growth rates of these various instability modes and discuss the inhibition of instabilities due to the angular dispersion of the beam. In all numerical calculations below, we fix $\xi_{\rm b} = 0.1$.

3.2 Oblique two-stream instability

The oblique two-stream instability corresponds to the Čerenkov resonance of the relativistic beam with the Langmuir modes of the background plasma. In the case of a magnetized background plasma, the electrostatic modes that are excited propagate along the background magnetic field. Since the treatment is similar, we focus here on the unmagnetized case.

To evaluate numerically the growth rate, we proceed as follows. We impose the resonance condition $k_\parallel = \omega_{\rm p}/(\beta_{\rm b}c)$ and look for

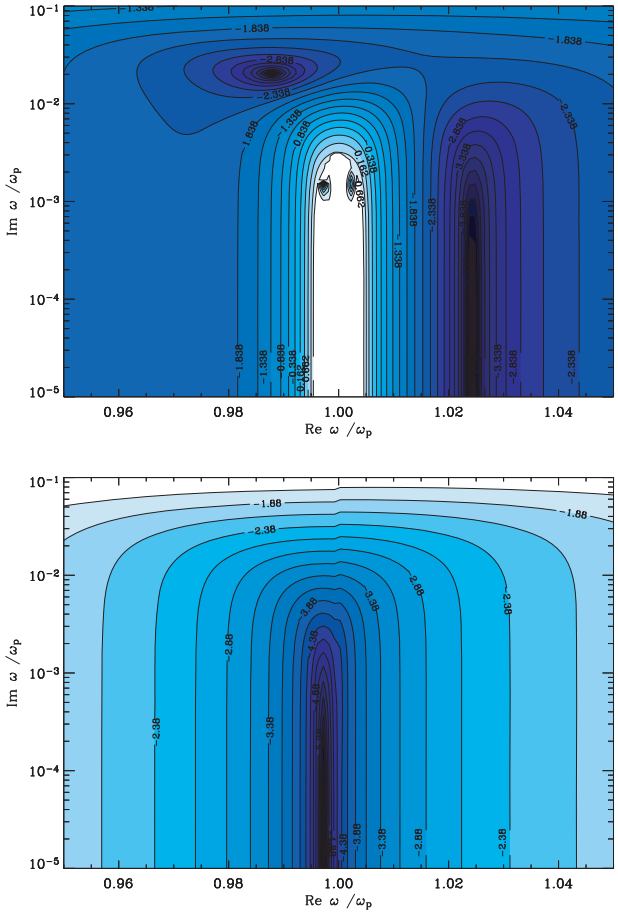

Figure 1. Contour map of the $\log_{10}$ of the left-hand side of the dispersion relation equation (4) for a cold background plasma, including the beam contribution. Top panel: $\gamma_{\rm b} = 10^5$, the electrostatic eigenmode includes one branch with zero imaginary part and one growing mode (as well as one decaying mode, not shown here), as indicated by the darker regions. Bottom panel: $\gamma_{\rm b} = 10^2$, the growing mode has disappeared due to the increased angular dispersion of the beam. In both plots, it is assumed $\omega_{\rm pb}^2/\omega_{\rm p}^2 = 0.1 m_{\rm e}/m_{\rm p}$, $k_\parallel = \omega_{\rm p}/(\beta_{\rm b}c)$ (resonance condition) and $k_\perp = \omega_{\rm p}/c$.

solutions of the full dispersion relation in the half plane ($\mathcal{R}\omega$, $\mathcal{I}\omega > 0$), including the beam contribution, for each given value of $k_\perp$. As the beam slightly modifies the real part of the root, this latter is slightly displaced from its unperturbed value $\omega_{\rm p}$. Fig. 1 offers an example of this procedure. It shows the locations of the roots of the dispersion relation in the $(\mathcal{R}\omega, \mathcal{I}\omega)$ plane for $\gamma_{\rm b} = 10^5$ (top panel) and $\gamma_{\rm b} = 10^2$ (bottom panel), with $k_\perp = \omega_{\rm p}/c$ in both cases. The growing mode is clearly seen in the top panel, but absent in the bottom panel in which the condition $k_\perp\beta_\perp c < \mathcal{I}\omega$ is violated due to the smaller value of $\gamma_{\rm b}$.

To leading order in $\chi^{\rm b}$, the growth rate reads (see Lemoine & Pelletier 2010)

$$\mathcal{I}\omega \simeq \frac{\sqrt{3}}{2^{4/3}}\left(\omega_{\rm pb}^2\omega_{\rm p}\right)^{1/3}\left(\frac{k_\perp^2c^2 + \omega_{\rm p}^2/\gamma_{\rm b}^2}{k_\perp^2c^2 + \omega_{\rm p}^2}\right)^{1/3}. \quad (6)$$

Therefore, the condition $k_\perp\beta_\perp c \ll \mathcal{I}\omega$ amounts to

$$\gamma_{\rm sh} \gg \xi_{\rm b}^{-1/3}\left(\frac{m_{\rm e}}{m_{\rm p}}\right)^{-1/3}\left(\frac{k_\perp c}{\omega_{\rm p}}\right)^{1/3} \qquad \left(\frac{\omega_{\rm p}}{\gamma_{\rm b}} \ll k_\perp c \ll \omega_{\rm p}\right). \quad (7)$$

One can thus check that, indeed, for $\gamma_{\rm sh} = 10$ (corresponding to $\gamma_{\rm b} \simeq 100$), the above condition is violated at $k_\perp c/\omega_{\rm p} = 1$, while it

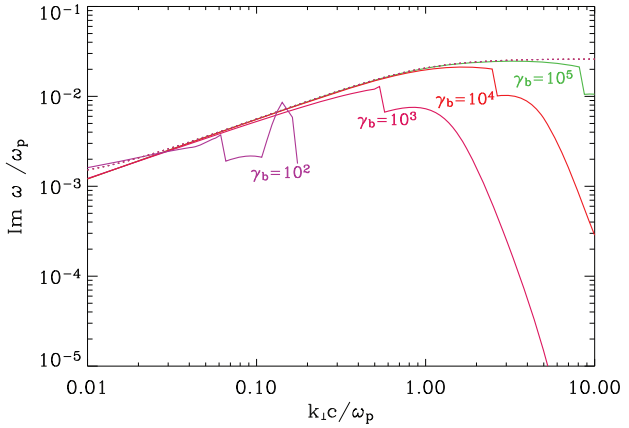

Figure 2. Growth rate of the oblique two-stream instability versus $k_\perp c/\omega_p$ for various values of γ_b: from left to right, $\gamma_b = 10^2, 10^3, 10^4, 10^5$. The cut-offs at high frequency are associated with the inhibition of growth due to angular dispersion of the beam; $\omega_{pb}^2/{\omega_p}^2 = 0.1 m_e/m_p$, $k_\parallel = \omega_p/(\beta_b c)$ (resonance condition). The dotted line shows the analytical solution to the growing mode (see Lemoine & Pelletier 2010).

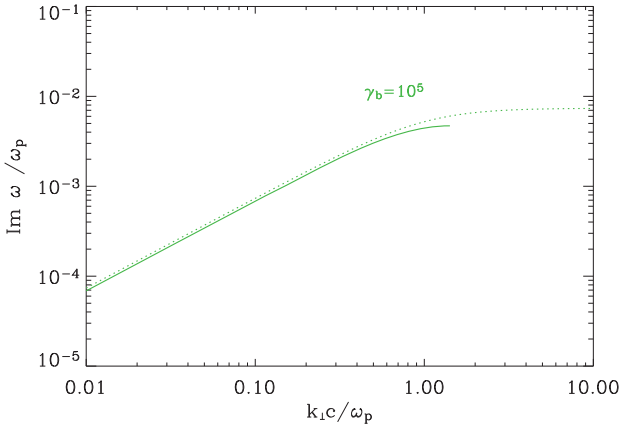

Figure 3. Same as Fig. 2, but for the filamentation instability. The calculation assumes $k_\parallel = 0$. Only the growth rate for $\gamma_b = 10^5$ is shown, as smaller values of γ_b did not lead to exact growing solutions.

is satisfied for $\gamma_{sh} = 300$ ($\gamma_b = 10^5$), in nice agreement with the numerical evaluations.

The effect of the beam temperature on the growth of the two-stream oblique instability has been discussed previously by Bret, Firpo & Deutsch (2005b) and Bret, Gremillet & Bénisti (2010), although in a slightly different context. They show that the two-stream instability is rather immune to angular dispersion contrary to the filamentation mode, as we find here, although the maximum growth rate of the oblique two-stream mode decreases with increasing dispersion; our findings also match these conclusions. In particular, as the angular dispersion increases, the maximum growth rate is found at smaller values of $k_\perp$, with a reduced growth rate.

Fig. 2 presents the numerical evaluation of the growth rate as a function of $k_\perp$ (solid line) for various values of γ_b (hence, various values of $u_\perp$). This figure clearly reveals the wavenumber cut-offs that correspond to the finite beam angular dispersion.

The smallest value of γ_{sh} that allows growth of the oblique two-stream instability corresponds to setting $k_\perp \to \omega_p/\gamma_b$ in equation (7), which leads to

$$\gamma_{sh} \gg \xi_b^{-1/5} \left(\frac{m_e}{m_p}\right)^{-1/5}. \tag{8}$$

Note that, at values $k_\perp \lesssim \omega_p/\gamma_b$, the oblique two-stream mode has reduced to the standard parallel two-stream instability. Furthermore, one must keep in mind that the above condition dictates whether growth may occur when angular dispersion is taken into account, yet for growth to occur, other conditions must be met. Most notably, the growth time-scale must be shorter than the precursor crossing time-scale. This latter condition depends on the degree of magnetization of the ambient medium, as discussed in detail in Lemoine & Pelletier (2010).

3.3 Filamentation instability

The filamentation instability appears at small values of $k_\parallel$ and $\mathcal{R}\omega$, as the solutions to the dispersion relation given in equation (4). The effect of the beam angular dispersion on the growth rate of the filamentation instability has been discussed by Bret et al. (2005b, 2010), and in the context of relativistic shocks by Lyubarsky & Eichler (2006) and recently by Rabinak et al. (2011). This instability turns out to be extremely sensitive to the beam angular dispersion, and as soon as $\gamma_b \lesssim 10^4$, the growth is inhibited for all values of $k_\perp$. One important difference relative to the oblique two-stream instability is the smaller growth rate of the filamentation instability, all things being equal, which implies that the condition $k_\perp \beta_\perp c > \mathcal{I}\omega$ is more easily satisfied at given values of γ_b and $k_\perp$. This is notably illustrated by Fig. 3, which shows the growth rate of the filamentation mode for various values of γ_b. This numerical calculation considers the limit $k_\parallel \to 0$ and finds the roots of the dispersion relation for various values of $k_\perp$, as before.

In detail, the growth rate of the filamentation instability in a cold background plasma is given at leading order by

$$\mathcal{I}\omega = \omega_{pb} \left(\frac{k_\perp^2 c^2}{k_\perp^2 c^2 + \omega_p^2}\right)^{1/2}, \tag{9}$$

therefore, $\mathcal{I}\omega \gg k_\perp \beta_\perp c$ implies

$$\gamma_{sh} \gg \xi_b^{-1/2} \left(\frac{m_e}{m_p}\right)^{-1/2} \qquad \left(k_\perp c \ll \omega_p\right), \tag{10}$$

independently of the value of $k_\perp$ as long as $k_\perp c \ll \omega_p$. At larger values of $k_\perp$, the right-hand side of equation (10) must be multiplied by $k_\perp c/\omega_p$ hence the condition is more stringent.

For $\xi_b = 0.1$, the numerical solution confirms that the filamentation instability disappears as soon as $\gamma_b \lesssim 10^4$, while it exists at wavenumbers shorter than ω_p/c for $\gamma_b = 10^5$. This agrees well with the above discussion.

4 INSTABILITIES IN A HOT BACKGROUND PLASMA WITH A FINITE BEAM ANGULAR DISPERSION

As discussed in some length in Section 2, one expects the incoming electrons to be heated to relativistic energies as they approach the shock front. Most notably, this preheating has been observed in various configurations in the latest PIC simulations of Sironi & Spitkovsky (2011). In particular, at low magnetization, the incoming upstream electrons carry about as much energy as the ions when they cross the shock transition. If half of the incoming proton kinetic energy density is transferred to the electron component and both electrons and protons retain a same bulk Lorentz factor, then one can easily show that the electrons are heated to a thermal Lorentz factor $\gamma_e \sim m_p/m_e$ in the electron fluid rest frame.

We thus consider here a hot electron background plasma, in the ultra-relativistic limit; we assume that the protons remain cold. We also retain the unmagnetized background plasma approximation and assume a ultra-relativistic Maxwellian distribution,

$$f_{\rm e}(\boldsymbol{p}) \,=\, n_{\rm e}\frac{c^3}{8\pi k_{\rm B}^3 T_{\rm e}^3}e^{-pc/k_{\rm B}T_{\rm e}}. \tag{11}$$

The longitudinal and transverse (with respect to $\boldsymbol{k}$) permittivities then read (e.g. Silin 1960; see also Hakim & Mangeney 1971; Melrose 1982; Braaten & Segel 1993; Bergman & Eliasson 2001)

$$\epsilon^{\rm L} \,=\, 1+\frac{\mu\omega_{\rm p}^2}{k^2c^2}\left[1+\frac{\omega}{2kc}\ln\left(\frac{\omega-kc}{\omega+kc}\right)\right], \tag{12}$$

$$\epsilon^{\rm T} \,=\, 1-\frac{\mu\omega_{\rm p}^2}{2k^2c^2}\left[1+\frac{\omega^2-k^2c^2}{2\omega kc}\ln\left(\frac{\omega-kc}{\omega+kc}\right)\right], \tag{13}$$

with $\gamma_{\rm e}=3/\mu$, $\mu=m_{\rm e}c^2/(k_{\rm B}T_{\rm e})$.

In what follows, the relativistic background plasma frequency is written as $\Omega_{\rm p}\,\equiv\,\omega_{\rm p}/\sqrt{\gamma_{\rm e}}$.

4.1 Two-stream instability

In the fully relativistic regime, the longitudinal mode has a refractive index smaller than unity for all values of k, hence the Čerenkov resonance with the unperturbed eigenmode can never be fully satisfied. In all rigor, one should derive the dispersion tensor allowing for corrections of order in $m_{\rm e}c^2/k_{\rm B}T$, as one is seeking a resonance at a refractive index of the order of $1/\beta_{\rm b}\simeq 1+1/(2\gamma_{\rm b})^2$ with a background plasma in which the mean Lorentz factor $\gamma_{\rm e}$ is much smaller than $\gamma_{\rm b}$. Such a dispersion tensor has been proposed by Braaten & Segel (1993). It takes the same form as that given in equations (12) and (13) although all kc must be replaced by kv_*, where v_* is an effective thermal velocity of electrons in the background plasma; hence $v_*\simeq\beta_{\rm e}c$. Then, one finds that the refractive index of the longitudinal mode becomes larger than unity (i.e. the dispersion relation crosses the light cone) at some value $k_*\simeq\sqrt{3}\,(\ln(4\gamma_{\rm e})-2)^{1/2}\,\omega_{\rm p}/c$. For $k\gtrsim k_*$, resonance is then possible. However, extrapolating the form of the dispersion tensor to the light-like region, one finds that the growth rate of the Čerenkov resonant mode with the unperturbed eigenmode is exponentially suppressed. We thus ignore this branch in the following.

Once the beam contribution to the dispersion relation is taken into account, one finds that an approximate resonance takes place for $\omega\simeq\Omega_{\rm p}$, $k_\parallel=\omega/\beta_{\rm b}c$ for small values $k_\perp\lesssim\Omega_{\rm p}/c$. This resonance solves exactly the dispersion relation and leads to growth of the modes. Neglecting the effect of angular dispersion, this can be understood analytically as follows.

The full dispersion relation reads

$$\left(\Lambda_{xx}+\chi^{\rm b}_{xx}\right)\left(\Lambda_{yy}+\chi^{\rm b}_{yy}\right)-\left(\Lambda_{xy}+\chi^{\rm b}_{yy}\right)^2\,=\,0, \tag{14}$$

with

$$\Lambda_{xx} \,=\, \frac{k_\parallel^2}{k^2}\epsilon^{\rm L}+\frac{k_\perp^2}{k^2}\epsilon^{\rm T}-\frac{k_\perp^2c^2}{\omega^2}, \tag{15}$$

$$\Lambda_{yy} \,=\, \frac{k_\perp^2}{k^2}\epsilon^{\rm L}+\frac{k_\parallel^2}{k^2}\epsilon^{\rm T}-\frac{k_\parallel^2c^2}{\omega^2}, \tag{16}$$

$$\Lambda_{xy} \,=\, \frac{k_\parallel k_\perp}{k^2}\left(\epsilon^{\rm L}-\epsilon^{\rm T}+\frac{k^2c^2}{\omega^2}\right). \tag{17}$$

Consider now the limit $k_\perp\ll\Omega_{\rm p}/c$, keeping in mind that resonance implies $k_\parallel\simeq\Omega_{\rm p}/c$. The dispersion relation then boils down to that of the longitudinal mode with

$$\epsilon^{\rm L}+\chi^{\rm b}_{xx}\,\simeq\,0. \tag{18}$$

We now use the form of the dispersion tensor proposed by Braaten & Segel (1993) and set $\omega=\beta_{\rm p}k_\parallel c(1+\delta)$, with $|\delta|\ll 1$ as is customary. In this limit, the longitudinal response reduces to

$$\epsilon^{\rm L}\,\simeq\,4+\frac{3}{2}\ln\left(\frac{1}{4\gamma_{\rm e}^2}+\frac{\delta-\epsilon_\perp}{2}\right), \tag{19}$$

where $\epsilon_\perp\equiv(k-k_\parallel)/k_\parallel=k_\perp^2/2k_\parallel^2\ll 1$. Then the dispersion relation is solved provided

$$\delta^2 \,=\, \frac{\omega_{\rm pb}^2}{\Omega_{\rm p}^2}\left(\frac{1}{\gamma_{\rm e}^2}+\frac{k_\perp^2c^2}{\Omega_{\rm p}^2}\right)\frac{1}{\epsilon^{\rm L}}. \tag{20}$$

Due to the smallness of the argument of the log in $\epsilon^{\rm L}$, the real part of $\epsilon^{\rm L}$ is negative, hence the dispersion relation admits growing solutions. The argument of the log depends on δ, hence the following solution

$$\mathcal{I}\omega\,\simeq\,0.3\frac{\omega_{\rm pb}}{\Omega_{\rm p}}\frac{k_\perp c}{\Omega_{\rm p}} \tag{21}$$

is valid up to a logarithmic correction (also assuming $k_\perp\gg\Omega_{\rm p}/\gamma_{\rm b}c$).

In the opposite limit $k_\perp\gg\Omega_{\rm p}/c$, one finds two branches: the Čerenkov resonance with $\omega\sim kc$, which is exponentially suppressed as mentioned above, and the continuation of the above approximate resonance, with $\omega\simeq k_\parallel c\simeq\Omega_{\rm p}$. This latter, however, is nothing but a form of filamentation instability, since it corresponds to $\mathcal{R}\omega\,\ll\,k_\perp c$ and $k_\parallel\ll k_\perp$. This branch will therefore be discussed in the section that follows (see in particular equation 28).

Let us discuss now the effect of angular dispersion, focusing on the Čerenkov resonance at $k_\perp c\,\ll\,\Omega_{\rm p}\simeq\mathcal{R}\omega\simeq k_\parallel c$. Using equation (21), one finds that angular dispersion can be neglected, i.e. $k_\perp\beta_\perp c\,\ll\,\mathcal{I}\omega$ provided

$$\gamma_{\rm e}\gamma_{\rm b}\,\gg\,100\xi_{\rm b}^{-1}\left(\frac{m_{\rm e}}{m_{\rm p}}\right)^{-1}, \tag{22}$$

independently of the value of $k_\perp$, as long as $k_\perp\ll\Omega_{\rm p}/c$. This inequality involves both the thermal Lorentz factor $\gamma_{\rm e}$ of the background plasma and the Lorentz factor of the beam $\gamma_{\rm b}\simeq\gamma_{\rm sh}^2$. Thus, growth can occur provided the temperature of the background plasma is sufficiently high; the corresponding threshold temperature scales as $\gamma_{\rm sh}^{-2}$.

Fig. 4 shows the results of a numerical evaluation of the growth rate as a function of $k_\perp$, for two different background temperatures, with in each case various values of the beam Lorentz factor. The agreement with equation (22) is found to be quite satisfactory: for $\gamma_{\rm e}=30$, the instability disappears at values $\gamma_{\rm b}\lesssim 10^4$, while for $\gamma_{\rm e}=300$, it exists down to values of $\gamma_{\rm b}\sim 10^3$. Note that the growth rate peaks at a value $k_\perp c\sim\omega_{\rm p}/\sqrt{\gamma_{\rm e}}=\Omega_{\rm p}$, as one should expect.

4.2 Filamentation instability

The filamentation instability in the hot background plasma can be recovered in the limit $\mathcal{R}\omega\rightarrow 0, k_\parallel c\rightarrow 0$. We thus write $\omega\equiv iw, k_\parallel=0$ and neglect for the purpose of analytical calculations the angular dispersion of the beam. This form of instability has been discussed recently in Achterberg & Wiersma (2007). The background plasma response can be approximated as

$$\epsilon^{\rm L}\,\simeq\,1+3\frac{\Omega_{\rm p}^2}{k_\perp^2c^2}+3i\frac{w^3\Omega_{\rm p}^2}{k_\perp^5c^5}, \tag{23}$$

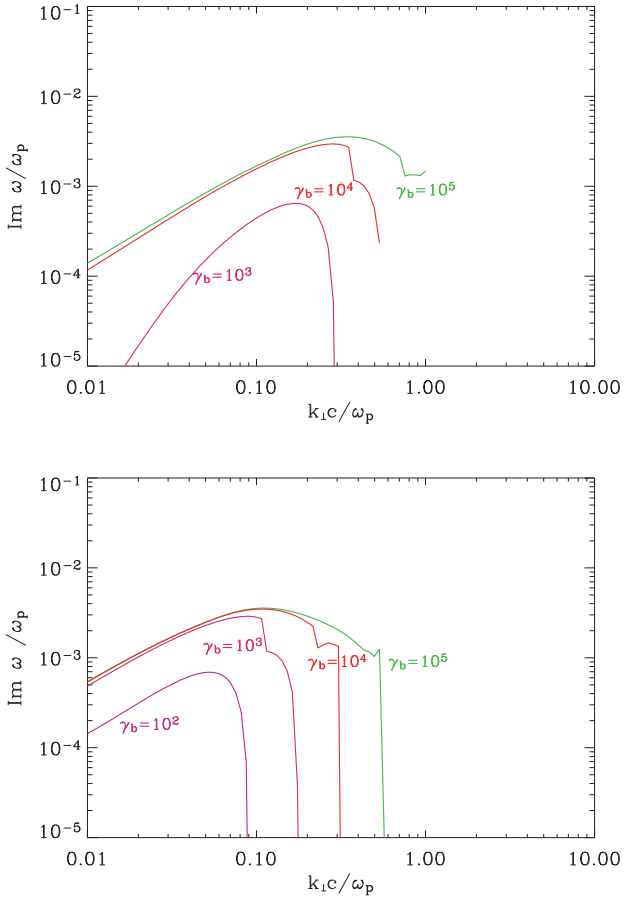

Figure 4. Growth rate of the two-stream instability in a relativistically hot background plasma versus $k_\perp c/\omega_\mathrm{p}$ (ω_p non-relativistic plasma frequency of the background plasma) for various values of γ_b at mean Lorentz factor $\gamma_\mathrm{e} = 30$ (top panel) and $\gamma_\mathrm{e} = 300$ (bottom panel) of the background plasma electrons. From left to right: $\gamma_\mathrm{b} = 10^3$ (bottom panel only), $\gamma_\mathrm{b} = 10^4, 10^5$. The calculation assumes $k_\parallel c = \Omega_\mathrm{p}/\beta_\mathrm{b}$.

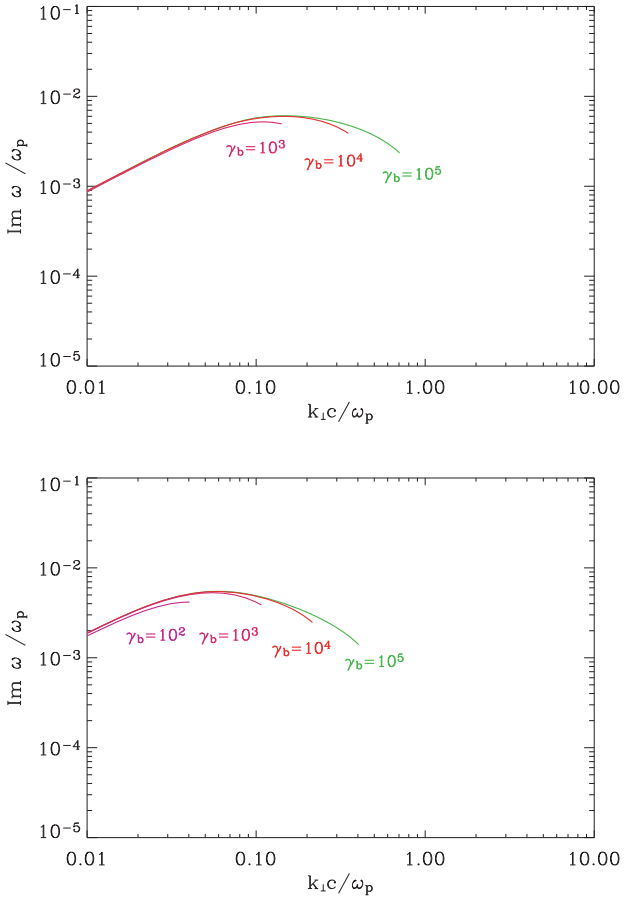

Figure 5. Same as Fig. 4 for the filamentation instability. The calculation assumes $k_\parallel = 0$. In the upper panel, $\gamma_\mathrm{e} = 30$ while in the lower panel, $\gamma_\mathrm{e} = 300$. From left to right: $\gamma_\mathrm{b} = 10^2$ (lower panel only), $\gamma_\mathrm{b} = 10^3, 10^4, 10^5$.

$$\epsilon^\mathrm{T} \simeq 1 + \frac{3\pi}{4}\frac{\Omega_\mathrm{p}^2}{k_\perp c w} - \frac{3i}{2}\frac{\Omega_\mathrm{p}^2 w}{k_\perp^3 c^3}. \tag{24}$$

Including the beam contribution, the dispersion relation equation (14) can be rewritten to leading order as

$$\left(1 + \frac{3\pi}{4}\frac{\Omega_\mathrm{p}^2}{k_\perp c w} + \frac{k_\perp^2 c^2}{w^2}\right)\left(1 + 3\frac{\Omega_\mathrm{p}^2}{k_\perp^2 c^2}\right) - 3\frac{\omega_\mathrm{pb}^2}{\Omega_\mathrm{p}^2}\frac{\Omega_\mathrm{p}^4}{w^4} \simeq 0. \tag{25}$$

We have implicitly assumed $k_\perp c \gg w$ in the above equation. Equation (25) can be solved in the three following limits.

If $k_\perp c \ll w^{1/3}\Omega_\mathrm{p}^{2/3}$, then $\Omega_\mathrm{p}^2/(k_\perp c w) \gg k_\perp^2 c^2/w^2 \gg 1$ and $\Omega_\mathrm{p}^2/{k_\perp}^2 c^2 \gg 1$, so that one obtains

$$\mathcal{I}\omega \simeq \left(\frac{4}{3\pi}\right)^{1/3}\left(\frac{\omega_\mathrm{pb}}{\Omega_\mathrm{p}}\right)^{2/3} k_\perp c \qquad \left(k_\perp c \ll \omega_\mathrm{pb}^{1/3}\Omega_\mathrm{p}^{2/3}\right). \tag{26}$$

The inequality written in parentheses corresponds to the assumption $k_\perp c \ll w^{1/3}\Omega_\mathrm{p}^{2/3}$.

If $\omega_\mathrm{pb}^{1/3}{\Omega_\mathrm{p}}^{2/3} \ll k_\perp c \ll \Omega_\mathrm{p}$, one rather obtains

$$\mathcal{I}\omega \simeq \omega_\mathrm{pb} \qquad \left(\omega_\mathrm{pb}^{1/3}\Omega_\mathrm{p}^{2/3} \ll k_\perp c \ll \Omega_\mathrm{p}\right), \tag{27}$$

which corresponds to the standard filamentation growth rate in a background plasma at high wavenumbers. The width of the band here is governed by $(\Omega_\mathrm{p}/\omega_\mathrm{pb})^{1/3} \simeq \gamma_\mathrm{e}^{-1/6}\xi_\mathrm{b}^{-1/6}(m_\mathrm{e}/m_\mathrm{p})^{-1/6}$. It should thus not be much larger than unity.

Finally, if $k_\perp c \gg \Omega_\mathrm{p}$, one finds

$$\mathcal{I}\omega \simeq \sqrt{3}\frac{\omega_\mathrm{pb}}{\Omega_\mathrm{p}}\frac{\Omega_\mathrm{p}}{k_\perp c} \qquad \left(\Omega_\mathrm{p} \ll k_\perp c\right). \tag{28}$$

Regarding the effect of angular dispersion, one finds that it can be safely neglected provided as before, $k_\perp \beta_\perp c \ll \mathcal{I}\omega$, or

$$\gamma_\mathrm{e}^{1/3}\gamma_\mathrm{b}^{1/2} \gg \xi_\mathrm{b}^{-1/3}\left(\frac{m_\mathrm{e}}{m_\mathrm{p}}\right)^{-1/3}, \tag{29}$$

assuming $k_\perp c \ll \omega_\mathrm{pb}^{1/3}\Omega_\mathrm{p}^{2/3}$.

Fig. 5 presents the result of a numerical evaluation of the filamentation growth rate in a relativistically hot background plasma, for various values of γ_b, taking into account the angular dispersion. In the left-hand panel, the mean background Lorentz factor is $\gamma_\mathrm{e} = 30$ while in the right-hand panel, $\gamma_\mathrm{e} = 300$. As expected the growth rate peaks at $k_\perp c \sim \Omega_\mathrm{p}$. The angular dispersion shuts off the filamentation instability at values of $k_\perp$ that scale with γ_b: indeed, in the range $k_\perp c \gg \Omega_\mathrm{p}$, the condition $k_\perp \beta_\perp c \ll \mathcal{I}\omega$ is much more restrictive, as the right-hand side of equation (29) is to be multiplied by $(k_\perp c/\Omega_\mathrm{p})^2$.

However, in contrast to the results for a cold background plasma shown in Fig. 3, the growth rate at small wavenumbers is not strongly affected by the angular dispersion. In this way, the relativistic temperature of the background sustends the filamentation instability at

small wavenumbers (relatively to Ω_p/c) and moderate values of the beam Lorentz factor.

4.3 Summary

Before turning to the current-driven instabilities, it may prove useful to briefly summarize the above results. We have discussed how the filamentation and the oblique two-stream instabilities are affected by the finite angular dispersion of the beam and the relativistic temperature of the electrons of the background plasma. In accordance with previous works (Lyubarsky & Eichler 2006; Rabinak et al. 2011), we find that the filamentation instability is strongly sensitive to the angular dispersion in a cold background plasma. For an electron–proton plasma, a Lorentz factor $\gamma_{\rm sh} \lesssim 100$ shuts off the filamentation instability in a cold background plasma due to the finite angular dispersion, the extent of which varies in inverse proportion to $\gamma_{\rm sh}$. Due to its higher growth rate, the oblique two-stream instability is much less sensitive to the finite angular dispersion and growth may take place at small wavenumbers for $\gamma_{\rm sh}$ as small as 10–20. As we have stressed, this does not take into account the limitation that is imposed by the size of the precursor: for the mode to actually grow in a shock precursor, its growth time-scale must also be smaller than the precursor crossing time. This latter condition is discussed in detail in Lemoine & Pelletier (2010) and, as it depends directly on the level of magnetization of the upstream plasma, we do not discuss it here for simplicity.

Once the electrons are heated to relativistic temperatures, the picture becomes substantially different. Then, the filamentation mode becomes rather insensitive to the angular dispersion at small wavenumbers, while the oblique two-stream instability is strongly inhibited. In both cases, the growth rate of the instability is maximal at a wavenumber $k_\perp \sim \Omega_p/c$, which varies as the inverse square root of the electron temperature. Conversely, a larger electron temperature implies a larger spatial scale for the mode of maximum growth rate.

5 CURRENT INSTABILITIES

Section 2.2 has discussed the possibility of current-driven instabilities at relativistic shocks. In particular, we have argued that a net parallel current in the beam of returning particles may emerge at oblique shock waves (in the upstream frame) if the electrons of the upstream plasma are not heated to equipartition with the protons by the time they are overtaken by the shock front. We have also indicated that, independently of charge neutralization of the returning beam, a net perpendicular current may rise through charge splitting in an external magnetic field. In the following, we discuss these possibilities in turn.

5.1 Parallel current

If the shock foot does not preheat the incoming electrons efficiently, a parallel current with typical (upstream rest frame) intensity

$$j_\parallel \sim \xi_{\rm b}\gamma_{\rm sh}^2 n_{\rm u} e c \tag{30}$$

rises in the shock precursor. Even if a substantial fraction of the incoming electrons were reflected at the shock front, the above current would rise, simply because these electrons would carry an energy $\sim m_{\rm e}/m_{\rm p}$ that of the reflected protons (in the absence of preheating), hence their penetration length-scale in the upstream would be very small compared to that of the protons.

This current gives rise to a compensating return current in the upstream plasma, which may destabilize the pre-existing magnetic field on large spatial scales (see Reville et al. 2007 for parallel relativistic shock waves).

It is interesting to note that, for realistic values of $\xi_{\rm b}$ and $\gamma_{\rm sh}$, the current exceeds $n_{\rm u}ec$, hence it cannot be simply compensated by a non-relativistic drift of the upstream electrons relatively to the ions. In order to understand how compensation takes place, it is instructive to go to the shock frame, in which the parallel current $j_{\parallel|{\rm sh}} = \xi_{\rm b}\gamma_{\rm sh} n_{\rm u} e c$ is associated with the charge density $\xi_{\rm b}\gamma_{\rm sh} n_{\rm u} e$. Note that the parallel current can be maintained in the shock front frame only if there is a net flow of particles escaping towards upstream; this therefore implicitly means a subluminal (parallel) shock configuration. Although the shock structure is not strictly speaking stationary in this case, we assume here that it evolves on long time-scales. In this frame, the incoming electrons and protons enter the precursor with the Lorentz factor $\gamma_{\rm sh}$ and density $\gamma_{\rm sh} n_{\rm u}$. If the electron fluid is suddenly slowed by an obstacle from velocity $\beta_{\rm sh}$ down to velocity $\beta_{\rm ex}$, its shock frame density jumps by a factor $\beta_{\rm sh}/\beta_{\rm ex}$ but the electron current $j_{\rm ex} = \gamma_{\rm ex}\beta_{\rm ex} n_{\rm ex} e c$ – which is positive as the electrons flow in the negative x direction – remains conserved. Therefore, the total incoming $e + p$ current must remain zero. Given that immediately before entering the precursor, the incoming $e + p$ current vanishes, while immediately within the precursor, the cosmic ray current does not vanish; it is easy to see that one cannot balance the current by simply slowing down the incoming electrons or protons.

In order to achieve charge and current neutralization within the precursor, it is actually necessary to reflect part of the electrons. Let us assume that a fraction $\kappa_{\rm e}$ is reflected back towards upstream at entrance into the precursor and that electrons and protons move with respective velocities $\beta_{\rm ex}$ and $\beta_{\rm px}$ within the precursor. The incoming proton current $j_{\rm px} = -\gamma_{\rm sh}\beta_{\rm sh} n_{\rm u} e c$, the incoming electron current $j_{\rm ex} = \gamma_{\rm sh}\beta_{\rm sh}(1-\kappa_{\rm e}) n_{\rm u} e c$, the incoming proton charge $\rho_{\rm px} = \gamma_{\rm px} n_{\rm px} e = \gamma_{\rm sh} n_{\rm u} e \beta_{\rm sh}/\beta_{\rm px}$ and the incoming electron charge $\rho_{\rm ex} = -\gamma_{\rm ex} n_{\rm ex}(1-\kappa_{\rm e}) e = -\gamma_{\rm sh} n_{\rm u}(1-\kappa_{\rm e}) e \beta_{\rm sh}/\beta_{\rm ex}$. Charge and current neutralization within the precursor thus requires

$$\kappa_{\rm e} = \xi_{\rm b}, \qquad \beta_{\rm ex} = \frac{\beta_{\rm sh}}{\xi_{\rm b} + \beta_{\rm sh}/\beta_{\rm px}}\,(1-\kappa_{\rm e})\,. \tag{31}$$

In this case, most of the compensating current in the background plasma is carried by the incoming protons, while the repelling and the slowing down of the electrons ensure charge balance. As the incoming protons are further decelerated by energy exchange with the incoming electrons through micro-instabilities, the above relation between $\beta_{\rm ex}$ and $\beta_{\rm px}$ must remain valid to preserve charge neutralization. Of course, $\xi_{\rm b}$ itself varies with location, decreasing roughly exponentially ahead of the shock front. Then, the above indicates that electrons are slowed down progressively as they cross the precursor; in the limit $\beta_{\rm px} \to \beta_{\rm sh}$, $\beta_{\rm ex} \to (1 - 2\xi_{\rm b})$, leading to efficient slowing down of the electrons.

Clearly, one should seek this effect in current PIC simulations. The PIC simulations of Sironi & Spitkovsky (2011) indicate that the generation of turbulence does not lead to efficient preheating of the electrons in the upstream. One may likely relate this to the magnetic nature of the modes excited by the Bell instability, which do not contain significant electric wave energy in the upstream frame. None the less, the precursor length-scale increases in time in the case of parallel shock waves, because a fraction of the accelerated particles can propagate to upstream infinity in such a configuration (Lemoine & Pelletier 2010). Hence, the structure of the precursor should itself evolve in time: as the length-scale of the precursor increases, incoming electrons experience heating for a longer duration and

arrive at the shock front with a larger fraction of the incoming ion energy; if this fraction eventually becomes comparable to unity, the upstream parallel current disappears and the Bell instability shuts off. Unfortunately, present PIC simulations have not been able to explore the evolution of the precursor on such long time-scales.

In the case of oblique shock waves, the simulations of Sironi & Spitkovsky (2011) indicate that the preheating of the electrons does not take place efficiently at intermediate magnetizations $10^{-4} \lesssim \sigma_{\rm u} \lesssim 10^{-2}$. There is no parallel current in this case in the shock frame, only a net charge as discussed in Pelletier et al. (2009). A priori, one might expect preheating to occur through a Buneman instability induced by the perpendicular current (see further below). However, as will be shown in Section 5.2, the magnetization is so large that the Buneman mode does not have time to grow before it is advected through the shock front, unless the shock Lorentz factor takes quite moderate values. Hence, it should not bear a significant impact on the structure of the precursor.

5.2 Current-induced Buneman instability

Let us assume that the accelerated particle beam carries a net current and induces a compensating return current in the background plasma. This situation applies equally well to the case of a parallel (Section 5.1) or a perpendicular current (Section 5.3). The relativistic motion of the background electrons relative to the background ions then induces a relativistic version of the Buneman instability (Buneman 1959).

In the upstream rest frame, the relevant dispersion relation, including the relativistic motion of the background electrons with velocity $\boldsymbol{v}_0$ (Lorentz factor γ_0) but neglecting the beam contribution, takes the form

$$1 - \frac{\omega_{\rm pi}^2}{\omega^2} - \frac{\omega_{\rm pe}^2}{\gamma_{\rm e}\left(\omega - \boldsymbol{k}\cdot\boldsymbol{v}_0\right)^2}\left[1 - \frac{\left(\boldsymbol{k}\cdot\boldsymbol{v}_0\right)^2}{k^2c^2}\right] = 0. \tag{32}$$

The instability develops at frequencies $|\omega| \ll \omega_0 \equiv \boldsymbol{k}\cdot\boldsymbol{v}_0$, as the small denominator lies in the second term, not the third one. Thus, we may approximate the dispersion relation as

$$1 - \frac{m_{\rm e}}{m_{\rm p}}\frac{\omega_{\rm pe}^2}{\omega^2} - \frac{\omega_{\rm pe}^2}{\omega_0^2}\frac{k_{\rm tr}^2}{k^2}\left(1 + 2\frac{\omega}{\omega_0}\right) \simeq 0, \tag{33}$$

where $k_{\rm tr} = [k^2 - (\boldsymbol{k}\cdot\boldsymbol{v}_0)^2]^{1/2}$ represents the component of $\boldsymbol{k}$ transverse to the current. The above expression then leads to the most unstable mode:

$$\omega_k \simeq \left(\frac{m_{\rm e}}{2m_{\rm p}}\right)^{1/3}\gamma_0^{-1/6}\left(\frac{k_{\rm tr}}{k}\right)^{1/3}\left(-\frac{1}{2} + i\frac{\sqrt{3}}{2}\right)\omega_{\rm p}. \tag{34}$$

$$\omega_0 \equiv \boldsymbol{k}\cdot\boldsymbol{v}_0 = \frac{\omega_{\rm pe}}{\sqrt{\gamma_0}}\frac{k_{\rm tr}}{k}. \tag{35}$$

As measured in the upstream frame, the advection time across the foot is $(\gamma_{\rm sh}\omega_{\rm ci})^{-1}$, with $\omega_{\rm ci} = eB_{\rm u}/(m_{\rm p}c)$ the proton cyclotron frequency in the background magnetic field. Thus the Buneman instability can effectively grow if $\mathcal{I}(\omega_k) \gg \gamma_{\rm sh}\omega_{\rm ci}$ which leads to a condition on the ambient magnetization, as in Lemoine & Pelletier (2010):

$$\sigma_{\rm u} \ll \left(\frac{m_{\rm p}}{m_{\rm e}}\right)^{1/3}\frac{1}{\gamma_{\rm sh}^2}, \tag{36}$$

neglecting the $\gamma_0^{1/6}$ dependence. This Buneman mode turns out to be the fastest instability, although the oblique two-stream mode does lie far behind as its growth condition is given by almost the same inequality, except that the right-hand side term is multiplied by $\xi_{\rm b}^{1/3}$. Nevertheless, it is well known (at least in the non-relativistic regime) that this Buneman instability saturates rapidly by heating the electrons to a temperature such that the anisotropy due to the electron current is drowned by the broadened distribution (i.e. $\bar{v}_{\rm e} \sim v_{\rm e}$ in non-relativistic regime, $\bar{v}_{\rm e}$ being the electron thermal velocity, and $\bar{\gamma}_{\rm e} \sim \gamma_{\rm e}$ in relativistic regime), in agreement with the discussion of Section 3. In practice, and if conditions permit it (notably, magnetization), this Buneman mode thus serves as an efficient source of electron heating. In turn, this helps the filamentation mode develop at moderate values of $\gamma_{\rm sh}$, which could not develop in a cold background plasma given the amount of angular dispersion of the beam, as discussed above.

5.3 Perpendicular current in a magnetic field

We now consider an oblique shock wave. In the shock front, the magnetic field lies perpendicular to the shock normal, to a good approximation; we assume that $\boldsymbol{B}_{\rm u|sh} = B_{\rm u|sh}\boldsymbol{y}$. As discussed in Section 2.1, the returning or accelerated proton undergoes a cycloidal trajectory in the Lorentz transformed background field and accompanying motional electric field, as measured in the shock front frame. Even if the beam does not carry a net parallel current at the beginning of the foot, the charge splitting in the background field leads to a cosmic ray current oriented along $\boldsymbol{z}$. Its magnitude in the upstream rest frame can be straightforwardly estimated as $j_{z,{\rm b}} \sim \xi_{\rm b}\gamma_{\rm sh}n_{\rm u}ec$, given that the apparent density of cosmic rays in this rest frame reads $\xi_{\rm b}\gamma_{\rm sh}^2 n_{\rm u}$ but that their effective perpendicular velocity is $v_z \sim c/\gamma_{\rm sh}$.

5.3.1 Magnetic field structure in the precursor

The vertical current tends to strongly modify the initial magnetic field in a diamagnetic way. Indeed, the choice of orientation of the field, directed towards $+y$, implies that the vertical current is directed towards $+z$, so that the magnetic field increases towards $+x$, from the shock ramp to the external edge of the foot where it reaches its external value. A consistent solution thus requires a reduced mean field in the foot. This remains fully compatible with the shock crossing conditions, which implies an enhancement of the magnetic field strength downstream, when one realizes that a similar current develops behind the shock over a distance measured by a typical Larmor radius. This current develops in an opposite direction downstream to that upstream and thus leads to a reduction of the magnetic field from its far downstream (asymptotic) value to the low value close to the ramp. Note that the cycloidal trajectories upstream and downstream have different characteristic gyroradii, due to the compression of the magnetic field.

This diamagnetic effect could be very prohibitive if the perpendicular current were not compensated by the background electrons. Indeed, in the absence of compensation, one would find an induced field $B_{\rm ind}$ such that

$$\frac{B_{\rm ind}\left(B_{\rm u|sh} - B_{\rm ind}\right)}{4\pi} \sim \xi_{\rm b}\gamma_{\rm sh}^2 n_{\rm u}m_{\rm p}c^2. \tag{37}$$

The modification of the magnetic profile can be calculated as follows. First we remark that the motional electric field that compensates $\beta_x B_y$ is uniform throughout the shock transition because rot $\boldsymbol{E} = 0$, hence $E_z = \beta_{\rm sh}B_{\rm u|sh}$. Then, in order to characterize the compensation of the current, we introduce an effective resistivity η of the background plasma electrons. At the tip of the precursor, where the beam current is the strongest, one cannot exclude that a

'double layer' type of structure forms, as in the case of a parallel shock wave. For the discussion that follows, we ignore this and describe the current compensation on phenomenological grounds by introducing this effective resistivity. In the precursor and in the shock ramp, this resistivity may result from turbulent scattering at frequency $\nu_{\rm e}$, with $\eta = 4\pi\nu_{\rm e}/\omega_{\rm pe}^2$. Ohm's law for the background plasma then leads to

$$\beta_{\rm sh} B_{\rm u|sh} + \beta_x B_y = \frac{\eta}{\gamma_{\rm sh}} j_{z,\rm pl}, \tag{38}$$

with $j_{z,\rm pl}$ the background plasma compensating current along z. Now the field variation is produced by both the plasma current $j_{z,\rm pl}$ and the diamagnetic cosmic ray current $j_{z,\rm b}$:

$$\frac{\partial B_y}{\partial x} = \frac{4\pi}{c}\left(j_{z,\rm pl} + j_{z,\rm b}\right). \tag{39}$$

Using Ohm's law to relate $j_{z,\rm pl}$ with B_y, one thus obtains the following differential equation that governs the spatial profile of the magnetic field:

$$\frac{\ell_{\rm r}}{\gamma_{\rm sh}}\frac{\partial B_y}{\partial x} - \beta_x B_y = \beta_{\rm sh} B_{\rm u|sh} + \frac{4\pi\ell_{\rm r}}{\gamma_{\rm sh} c} j_{z,\rm b}, \tag{40}$$

where $\ell_{\rm r}$ denotes the resistive length, $\ell_{\rm r} \equiv \eta c/4\pi = \delta_{\rm e}^2 \nu_s/c$. The boundary conditions are as follows: for $x \to -\infty$ (far downstream), $\beta_x \to -1/3$, the current vanish and $B_y \to 3B_{\rm u|sh}$; for $x \to +\infty$ (far upstream), $\beta_x \to -\beta_{\rm sh} \simeq -1$, the currents vanish again and $B_y \to B_{\rm u|sh}$. In the downstream region in which there is a cosmic ray current $j_{z,\rm b} < 0$, B_y decreases below $3B_{\rm u|sh}$; correspondingly, in the upstream region in which $j_{z,\rm b} > 0$, B_y increases towards its asymptotic value $B_{\rm u|sh}$.

In the situation that we consider, the magnetic field energy is weak and the incoming plasma is able to provide a compensating current. The typical length-scale over which the compensating current is established, $\ell_{\rm r}$, is much smaller than the length-scale over which the cosmic ray current is induced $\ell_{\rm f|sh}$, hence one derives the modification of the magnetic field at $x > \ell_{\rm r}$ as $B_y = B_{\rm u|sh} + \Delta B^+$ with

$$\Delta B^+ \simeq -\frac{4\pi\ell_{\rm r}}{\gamma_{\rm sh}\beta_{\rm sh} c} j_{z,\rm b}, \tag{41}$$

and the compensating current

$$j_{z,\rm pl} = \frac{c}{4\pi}\frac{\partial B_y}{\partial x} - j_{z,\rm b} = -\left(1 + \frac{\ell_{\rm r}}{\gamma_{\rm sh}}\frac{\partial}{\partial x}\right) j_{z,\rm b}. \tag{42}$$

The discrepancy with respect to neutralization of the diamagnetic current is expressed by the derivative term in the above expression, and is of the order of $\ell_{\rm r}/\gamma_{\rm sh}\ell_f$. Thus, the diamagnetic current upstream produces a modification of the magnetic field of a maximum amount given by

$$\frac{\Delta B^+}{B_{\rm u|sh}} \sim \frac{4\pi\ell_{\rm r} n_{\rm b} c}{\gamma_{\rm sh} B_{\rm u|sh}} \sim 4\pi\xi_{\rm b}\gamma_{\rm sh}^{-1}\frac{\ell_{\rm r}}{\delta_{\rm e}}\sigma_{\rm u}^{-1/2}\left(\frac{m_{\rm e}}{m_{\rm p}}\right)^{-1/2}. \tag{43}$$

The modification thus remains small if

$$\sigma_{\rm u} \gtrsim \xi_{\rm b}^2\left(\frac{m_{\rm e}}{m_{\rm p}}\right)\gamma_{\rm sh}^{-2} \sim 10^{-10}. \tag{44}$$

The right-hand side is of the order of $10^{-6}\gamma_{\rm sh}^{-2}$, hence it should be verified in most relevant cases.

The above transverse current leads to a compensating current in the background plasma which induces a Buneman instability, as discussed in Section 5.2. As the beam transverse current is generated at the tip of the precursor, where most of the rotation in the background field takes place, the Buneman instability effectively takes place in a cold background plasma. It may then lead to efficient heating of the electrons, as discussed in Section 5.2.

6 DISCUSSION AND CONCLUSIONS

The present work has discussed the electromagnetic microinstabilities triggered by a beam of shock-reflected/accelerated particles propagating in the unshocked upstream plasma. In particular, it has taken into account the finite angular dispersion of the beam of returning particles as well as the possible effects of heating of the background plasma electrons. Regarding the development of the filamentation and two-stream instabilities, the salient results are summarized in Section 4.3. Let us discuss here how these results affect our understanding of the development of instabilities at ultra-relativistic shock waves, as a function of the shock Lorentz factor $\gamma_{\rm sh}$.

(1) At large values of $\gamma_{\rm sh} \gtrsim 300$, both the filamentation and modified two-stream instabilities can develop in the cold or relativistically hot background plasma limits. As mentioned earlier, this statement only considers the effect of angular dispersion and plasma temperature. For the waves to actually grow, one must satisfy another condition: the growth time-scale must be shorter than the precursor crossing time-scale. This latter condition depends on the magnetization of the upstream plasma and is discussed in detail in Lemoine & Pelletier (2010). In the rest of this discussion, we do not consider this limitation, which amounts to considering a very weakly magnetized upstream plasma.

(2) At lower values of $\gamma_{\rm sh}$, the filamentation instability is inhibited by the finite angular dispersion of the beam – the extent of which is inversely proportional to $\gamma_{\rm sh}$ – in the cold background plasma limit, but not in the relativistically hot background plasma limit. The oblique two-stream instability is inhibited in the hot background plasma limit, at least up to some threshold temperature which scales as $\gamma_{\rm sh}^{-2}$ (see equation 22).

(3) We have uncovered a situation that leads to the development of a Buneman instability at the tip of the precursor, which may efficiently preheat the electrons to relativistic temperatures. The Buneman instability is usually triggered by a parallel current. But, for the generic case of an oblique relativistic shock wave, the rotation of the beam in the background magnetic field leads to a perpendicular current of large intensity. This leads to a compensating transverse current in the background plasma, which in turn leads to the Buneman instability, possibly in the relativistic regime. As is well known, this instability saturates through the heating of the electrons such that the thermal energy becomes comparable with the drift energy, thereby drowning the anisotropy of the electron distribution. The growth rate of the Buneman instability is larger than that of the oblique two-stream instability or the filamentation mode in the cold background zero angular dispersion limit.

(4) The above then suggests that efficient preheating of the upstream electrons may take place through the Buneman instability and through the two-stream instability. As soon as the electrons are heated to relativistic temperatures, the filamentation instability becomes the dominant mode. As indicated by equation (29), this instability can indeed operate down to values $\gamma_{\rm sh} \sim 10$ in the relativistically hot background plasma limit. For smaller values of $\gamma_{\rm sh}$, the ultra-relativistic shock limit that we have assumed throughout is no longer applicable. One should expect different physics to come into play in the mildly relativistic limit.

The upstream electrons are heated to larger thermal Lorentz factors $\gamma_{\rm e}$ as they come closer to the shock front, hence the above picture must pertain up to the shock front. If the electron temperature reaches the threshold discussed previously, the two-stream

instability also becomes efficient. For reference, if the electrons reach equipartition with the protons, γ_e becomes as large as m_p/m_e. At equipartition, the filamentation instability thus becomes similar to that occurring in a pair plasma. As for the Whistler wave instability, it develops only if there is a sufficient contrast between the electron and proton masses. It thus disappears when the electron relativistic mass reaches the proton mass and the modes become right Alfvén waves, which do not have time to grow unless the precursor has been substantially extended through diffusion (see the discussion in Lemoine & Pelletier 2010).

(5) The typical perpendicular spatial scale at which the filamentation and two-stream instability growth rates reach their maximum scales as $\sqrt{\gamma_e}$ due to the evolution of the background plasma frequency in the ultra-relativistic limit. This suggests that the typical spatial scale of the inhomogeneities increases from the electron inertial scale c/ω_{pe} to the proton inertial scale c/ω_{pi} as the modes come closer to the shock front. Note that the growth rate of the filamentation instability does not depend on the temperature of the background plasma and takes the same value as in the cold plasma limit.

(6) The micro-turbulence that is generated by these instabilities leads to efficient electron heating. This has been discussed in Section 2.2, where it has been argued, in particular, that in the unmagnetized limit, the large scale of the precursor must guarantee heating of the electrons to equipartition with the protons if the wave electric energy content is comparable to the magnetic content. Let us now account for a finite upstream magnetic field, assuming in particular that this magnetic field sets the length-scale of the precursor. The heating process takes place through the diffusion of the electron energy in the bath of micro-turbulence: in fluctuating electric fields $\bar{E}$ on coherence scales l_c, electrons reach a thermal energy $\bar{\epsilon}_e$ such that $\bar{\epsilon}_e^2 \simeq 2e^2\bar{E}^2 l_c \ell_{f|u}$ after crossing the precursor of length $\ell_{f|u}$. The turbulence is supposed to reach a level such that it contributes to form the shock, i.e. $\bar{E}^2/(4\pi) = \xi_E n_u m_p c^2$ with ξ_E being a conversion factor not too far below unity. This implies a thermal energy $\bar{\epsilon}_e \sim \xi_E^{1/2}\sigma_u^{-1/4}\gamma_{sh}^{-1/2} m_p c^2$. For fiducial values $\xi_E \sim 10^{-2}$, $\sigma_u \sim 10^{-9}$, $\gamma_{sh} \sim 300$, the prefactor is of the order of unity. If one imposes furthermore that the magnetization is small enough to guarantee the growth of the filamentation mode, one finds $\sigma_u < \xi_b/\gamma_{sh}^2$ (Lemoine & Pelletier 2010), the electrons are heated to Lorentz factors $\gamma_e \gtrsim \xi_E^{1/2}\xi_b^{-1/4} m_p/m_e$, close again to equipartition.

Thus, the electrons can be heated in the precursor and roughly thermalized with the protons.

(7) The above considerations agree well with recent PIC simulations, at least where comparison can be made. In particular, electron heating to near equipartition has been observed at small magnetization by Sironi & Spitkovsky (2011), although the detailed physical process that is responsible for this heating has not been identified in these simulations. The micro-instabilities have been observed to take place at moderate values of the shock Lorentz factor $\gamma_{sh} \sim 20$ and small magnetization $\sigma_u \lesssim 10^{-4}$ (assuming in these simulations an electron-to-proton mass ratio of 1/16). Furthermore, the typical scale of the fluctuations apparently grows from the tip of the precursor to the shock front.

(8) Finally, we question the possible non-linear saturation of the instabilities in the precursor. First of all, one can show that these instabilities cannot be saturated by beam particle trapping because the time-scale to cross a coherence scale l_c is much less than the growth time-scale of the waves $\mathcal{I}\omega^{-1}$; in other words, trapping of the beam particles would require a prohibitive level of turbulence. This can be seen best by going to the rest frame of the waves in which the electromagnetic fields are static. In this rest frame, the particle crosses the transverse coherence length l_c in a time-scale $\tau_{nl|w} = (p_{b|w} l_c/e\bar{E}_{|w})^{1/2}$, which takes into account the static force exerted by the fields on the particle in this rest frame. As we are interested in the transverse dynamics, one can transform the relevant quantities to the upstream frame as $\tau_{nl|u} = \gamma_{w|u}\tau_{nl|w}$, $p_{b|w} \simeq p_b \simeq \gamma_{sh}^2 m_p c$ and $E_{|w} \simeq \gamma_{w|u}\bar{E}$. Consider now the example of the filamentation instability, the growth rate of which is $\xi_b^{1/2}(m_e/m_p)^{1/2}\omega_p$. Saturation by trapping would require $\xi_E \gtrsim \gamma_{w|u}^2 \xi_b^2 \gamma_{sh}^4 (l_c/\delta_p)^2$, which is obviously prohibitive. This negative conclusion obviously holds equally well for the other instabilities that grow faster, in particular the two-stream instability, the Whistler mode and the Buneman instability.

Non-linear effects related to mode coupling thus appear more likely. Even when the electrons have turned relativistically hot, the rate of non-linear evolution of the unstable modes – as for instance coupling of oblique two-stream modes with transverse waves or acoustic waves – is expected to be of the order of $\omega_{pe}\bar{E}^2/(4\pi\gamma_e m_e c^2)$ according to Zakharov (1972), which leads to saturation once the growth rate is balanced by the rate of energy conversion into the other stable modes. For the particular example of the two-stream instability, with growth rate $\xi_b^{1/3}(m_e/m_p)^{1/3}\omega_p$, this leads to $\xi_E \sim \xi_b^{1/3}(m_e/m_p)^{4/3}\gamma_e$, which is therefore not far below ξ_b if the electrons have reached equipartition with the ions. As a note of caution, one should point out that the above estimates of saturation ignore a possible bulk Lorentz factor of the upstream electrons once they have been heated in the precursor. Such estimates should nevertheless remain correct in the limit of moderate γ_{sh}.

The main conclusion of this study of the dispersion and of the thermal effects on the growth of micro-instabilities in the foot of a relativistic shock is that electron preheating can occur, and that this leads to the attenuation of micro-instabilities except the filamentation instability, which keeps the same growth rate, the wavelength of the instability peak migrating from the electron to the proton inertial scale as the electrons are heated to equipartition. The plasma that reaches the shock ramp is roughly thermalized and behaves like an electron–positron plasma. Hence the following question arises: what makes the reflection of a part of the incoming particles? Under the assumed conditions of a weak magnetization, such that it allows the growth of micro-instabilities, especially the filamentation instability, the role of the ponderomotive force exerted by the growing waves is probably more important than the electrostatic barrier. This has to be further investigated with dedicated PIC simulations.

ACKNOWLEDGMENTS

We acknowledge fruitful discussions with A. Spitkovsky and L. Sironi during the preparation of this work, as well as with I. Rabinak and E. Waxman. One of us, GP, is very grateful for the hospitality of the Kavli Institute for Theoretical Physics in Santa Barbara during the Summer Program of 2009 devoted to these topics; this was indeed a great opportunity for developing a better understanding that has influenced this paper and others to come, thanks to intense exchanges with many colleagues. We acknowledge support from the CNRS PEPS/PTI Program of the Institute of Physics (INP) and from the GDR PCHE.

REFERENCES

Achterberg A., Wiersma J., 2007, AA, 475, 19
Achterberg A., Gallant Y., Kirk J. G., Guthmann A. W., 2001, MNRAS, 328, 393

Achterberg A., Wiersma J., Norman C. A., 2007, AA, 475, 1
Akhiezer A. I., 1975, Plasma Electrodynamics. Pergamon Press, Oxford
Begelman M. C., Kirk J. G., 1990, ApJ, 353, 66
Bell A., 2004, MNRAS, 353, 550
Bergman J., Eliasson B., 2001, Phys. Plasmas, 8, 1482
Braaten E., Segel D., 1993, Phys. Rev. D, 48, 1478
Bret A., 2009, ApJ, 699, 990
Bret A., Firpo M.-C., Deutsch C., 2005a, Phys. Rev. Lett., 94, 115002
Bret A., Firpo M.-C., Deutsch C., 2005b, Phys. Rev. E, 72, 016403
Bret A., Gremillet L., Bénisti D., 2010, Phys. Rev. E, 81, 036402
Buneman O., 1959, Phys. Rev., 115, 503
Gallant Y., Achterberg A., 1999, MNRAS, 305, L6
Gedalin M., Balikhin M. A., Eichler D., 2008, Phys. Rev. E, 77, 026403
Gruzinov A., Waxman E., 1999, ApJ, 511, 852
Hakim R., Mangeney A., 1971, Phys. Fluids, 14, 2751
Hoshino M., 2008, ApJ, 672, 940
Langdon A. B., Arons J., Max C. E., 1988, Phys. Rev. Lett., 61, 779
Lemoine M., Pelletier G., 2010, MNRAS, 402, 321
Lemoine M., Pelletier G., Revenu B., 2006, ApJ, 645, L129
Li Z., Zhao X.-H., 2011, J. Cosmol. Astropart. Phys., 5, 008
Li Z., Waxman E., 2006, ApJ, 651, L328
Lyubarsky Y., 2006, ApJ, 652, 1297
Lyubarsky Y., Eichler D., 2006, ApJ, 647, L1250
Medvedev M. V., Loeb A., 1999, ApJ, 526, 697
Melrose D. B., 1982, Aust. J. Phys., 35, 41
Melrose D. B., 1986, Instabilities in Space and Laboratory Plasmas. Cambridge Univ. Press, Cambridge
Milosavlejvić M., Nakar E., 2006, ApJ, 651, 979
Niemiec J., Ostrowski M., 2006, ApJ, 641, 984
Pelletier G., Lemoine M., Marcowith A., 2009, MNRAS, 393, 587
Rabinak I., Katz B., Waxman E., 2011, ApJ, 736, 157
Reville B., Kirk J. G., Duffy P., 2006, Plasma Phys. Contr. Fus., 48, 1741
Silin V. P., 1960, Soviet Phys. JETP, 11, 1136
Sironi L., Spitkovsky A., 2009, ApJ, 698, 1523
Sironi L., Spitkovsky A., 2011, ApJ, 726, 75
Spitkovsky A., 2008a, ApJ, 673, L39
Spitkovsky A., 2008b, ApJ, 682, L5
Wiersma J., Achterberg A., 2004, AA, 428, 365
Zakharov V., 1972, Soviet JETP, 35, 908

APPENDIX A: BEAM SUSCEPTIBILITY TENSOR

The susceptibility tensor is written as (Melrose 1986):

$$\chi^{\rm b}_{ij} = \frac{4\pi n_{\rm b} e^2}{m\omega^2} \int {\rm d}^3 u \left[\frac{u_i}{\gamma} \frac{\partial}{\partial u_j} f_{\rm b} + \frac{u_i u_j}{\gamma} \frac{1}{\gamma\omega - k_m u_m c + i\epsilon} k_l c \frac{\partial}{\partial u_l} f_{\rm b} \right], \quad \text{(A1)}$$

with $u_i \equiv p_i/(mc)$, $\gamma \simeq (1+u_x^2)^{1/2}$ in the above equation and $n_{\rm b}$ the beam density (in the upstream plasma rest frame). We recall the axisymmetric waterbag distribution function adopted here:

$$f_{\rm b}(\boldsymbol{u}) = \frac{1}{\pi u_\perp^2} \delta\left(u_x - u_\parallel\right) \Theta(u_\perp^2 - u_y^2 - u_z^2). \quad \text{(A2)}$$

The integral in equation (A1) can be carried out analytically under the approximation discussed in Section 3: we neglect in a systematic way u_y^2 and u_z^2 in front of u_x^2 but we do not to neglect u_y, u_z in the poles of the form $\omega - \boldsymbol{k}\cdot\boldsymbol{\beta} c = \omega - k_i u_i c/\gamma_{\rm b}$. For simplicity, we rotate the perpendicular axes in such a way as to align the perpendicular component of the wave vector along y, i.e. $\boldsymbol{k}_\perp = k_\perp \boldsymbol{y}$. One then obtains

$$\chi^{\rm b}_{xx} = \frac{\omega_{\rm pb}^2}{\omega^2} \left\{ -\frac{1}{\gamma_{\rm b}^2} - 2k_\parallel u_\parallel \left[\left[\left(2-\beta_{\rm b}^2\right) \frac{1}{R_\parallel} + \frac{u_\parallel}{\gamma_{\rm b}} \frac{S_\parallel}{R_\parallel^2} \right] \mathcal{P}_{xx1}(z) - \frac{u_\parallel}{\gamma_{\rm b}} \frac{S_\parallel}{R_\parallel^2} \mathcal{P}_{xx2}(z) \right] + 2\frac{u_\parallel^2 k_\perp^2 c^2}{R_\parallel^2} \mathcal{P}_{xx3}(z) \right\}, \quad \text{(A3)}$$

$$\chi^{\rm b}_{xy} = \frac{\omega_{\rm pb}^2}{\omega^2} \left\{ -2\frac{k_\parallel}{k_\perp} \left[\left(\frac{1}{\gamma_{\rm b}^2} + 2\frac{u_\parallel}{\gamma_{\rm b}} \frac{S_\parallel}{R_\parallel} \right) \mathcal{P}_{xy1}(z) + \frac{u_\parallel}{\gamma_{\rm b}} \frac{S_\parallel}{R_\parallel} \mathcal{P}_{xy2}(z) \right] + 2\frac{u_\parallel k_\perp c}{R_\parallel} \mathcal{P}_{xy3}(z) \right\}, \quad \text{(A4)}$$

$$\chi^{\rm b}_{yx} = \chi^{\rm b}_{xy} \quad \text{(A5)}$$

$$\chi^{\rm b}_{xz} = \chi^{\rm b}_{xz} = 0, \quad \text{(A6)}$$

$$\chi^{\rm b}_{yy} = \frac{\omega_{\rm pb}^2}{\omega^2} \left\{ -1 - 2\frac{k_\parallel}{k_\perp} \left[\left(-\frac{u_\parallel}{\gamma_{\rm b}^2} \frac{R_\parallel}{k_\perp c} + 3\frac{S_\parallel}{k_\perp c \gamma_{\rm b}} \right) \mathcal{P}_{yy1}(z) + \frac{S_\parallel}{k_\perp c \gamma_{\rm b}} \mathcal{P}_{yy2}(z) \right] + 2\mathcal{P}_{yy3}(z) \right\}, \quad \text{(A7)}$$

$$\chi^{\rm b}_{zz} = \frac{\omega_{\rm pb}^2}{\omega^2} \left\{ -1 - 2\frac{k_\parallel}{k_\perp} \left[\left(-\frac{u_\parallel}{\gamma_{\rm b}^2} \frac{R_\parallel}{k_\perp c} + 3\frac{S_\parallel}{k_\perp c \gamma_{\rm b}} \right) \mathcal{P}_{zz1}(z) - \frac{S_\parallel}{k_\perp c \gamma_{\rm b}} \mathcal{P}_{zz2}(z) \right] + 2\mathcal{P}_{zz3}(z) \right\}, \quad \text{(A8)}$$

$$\chi^{\rm b}_{yz} = \chi^{\rm b}_{yz} = 0, \quad \text{(A9)}$$

with

$$z \equiv \frac{k_\perp u_\perp c}{R_\parallel},$$
$$R_\parallel \equiv \gamma_{\rm b}\omega - k_\parallel u_\parallel c,$$
$$S_\parallel \equiv u_\parallel \omega - k_\parallel \gamma_{\rm b} c. \quad \text{(A10)}$$

The beam plasma frequency is defined as usual: $\omega_{\rm pb} \equiv [4\pi n_{\rm b} e^2/(\gamma_{\rm b} m)]^{1/2}$. The beam velocity $\beta_{\rm b} = u_\parallel/\gamma_{\rm b}$.

$$
\begin{aligned}
\mathcal{P}_{xx1}(z) &= z^{-2}\left[1-(1-z^2)^{1/2}\right],\\
\mathcal{P}_{xx2}(z) &= (1-z^2)^{-1/2},\\
\mathcal{P}_{xx3}(z) &= z^{-2}\left[1-(1-z^2)^{-1/2}\right],\\
\mathcal{P}_{xy1}(z) &= z^{-2}\left[1-\frac{z^2}{2}-(1-z^2)^{1/2}\right],\\
\mathcal{P}_{xy2}(z) &= 1-(1-z^2)^{-1/2},\\
\mathcal{P}_{xy3}(z) &= \mathcal{P}_{xx3}(z),\\
\mathcal{P}_{yy1}(z) &= \mathcal{P}_{xy1}(z),\\
\mathcal{P}_{yy2}(z) &= \mathcal{P}_{xy2}(z),\\
\mathcal{P}_{yy3}(z) &= z^{-2}\left[1+\frac{z^2}{2}-(1-z^2)^{-1/2}\right],\\
\mathcal{P}_{zz1}(z) &= \frac{z^{-2}}{3}\left[-1+\frac{3z^2}{2}+(1-z^2)^{3/2}\right],\\
\mathcal{P}_{zz2}(z) &= -\mathcal{P}_{xx1}(z),\\
\mathcal{P}_{zz3}(z) &= \left[1-(1-z^2)^{1/2}\right].
\end{aligned}
\tag{A11}
$$

The above are defined for $k_\perp u_\perp c < |R_\parallel|$. In the opposite limit, i.e. when the effects of angular dispersion become substantial, the integral in equation (A1) contains poles. Using the Plemelj–Sohotsky formula to evaluate the integrals over these resonance poles, one finds that the above equations (A3, A4, A6, A7, A8, A9) for the beam susceptibility tensor are continued to the region $k_\perp u_\perp c > |R_\parallel|$ by the substitution $(1-x^2)^{1/2} \to i\,(x^2-1)^{1/2}$, with $x = k_\perp u_\perp c/R_\parallel$ in the expressions for the $\chi^{\rm b}_{ij}$ components.

This paper has been typeset from a TEX/LATEX file prepared by the author.